Electrochimica Acta 117 (2014) 504–520

Contents lists available at ScienceDirect

Electrochimica Acta

journal homepage: www.elsevier.com/locate/electacta

Using different chemical methods for deposition of CdS on TiO_2 surface and investigation of their influences on the dye-sensitized solar cell performance

Mohammad Sabet, Masoud Salavati-Niasari*, Omid Amiri

Institute of Nano Science and Nano Technology, University of Kashan, Kashan, P. O. Box. 87317–51167, Islamic Republic of Iran

ARTICLE INFO

Article history:
Received 21 September 2013
Received in revised form
20 November 2013
Accepted 23 November 2013
Available online 11 December 2013

Keywords:
CdS
Chemical methods
DSSC
Solar cell
Deposition

ABSTRACT

Electrophoresis deposition (EPD) was used for fabrication of TiO_2 layer on the FTO glass substrate. Different chemical methods such as successive ion layer adsorption and reaction (SILAR), chemical bath deposition (CBD), microwave (MW) and hydrothermal (HT) were served to deposition of CdS on the prepared TiO_2 surface. Also TiO_2/CdS nanocomposite was synthesized by hydrothermal method and was then deposited on the FTO surface via doctor balde (DB) technique. The effect of deposition method on optical properties was investigated. The results showed that different deposition methods create different electrodes with various optical properties. The surfaces was characterized by X-ray diffraction (XRD), transmission electron microscopy (TEM), scanning electron microscopy (SEM), cross-section SEM, UV-Vis diffuse reflectance spectroscopy (DRS), energy dispersive X-ray analysis (EDX) spectroscopy, atomic force microscopy (AFM), cyclic voltammetry (CV) and UV–vis spectroscopy. Dye-sensitized solar cells (DSSC) made by the fabricated electrodes as working electrode and then investigated by current density-voltage (J-V) curve and electrochemical impedance spectroscopic (EIS). It was found that deposition method has significant role in solar cell performance and efficiency.

1. Introduction

Dye-sensitized solar cells (DSCs) are currently attracting worldwide scientific and technological interest because of its high energy conversion efficiency [1–3] and simple fabrication process. Titanium dioxide (TiO_2), a wide band-gap (3.0–3.2 eV) semiconductor, is one of the most prominent oxide materials for performing various kinds of industrial applications such as photovoltaic [2], photocatalytic [4,5], photonic crystals [6], photochromic [7,8]. The band gap of TiO_2 (3.2 eV) limits its absorption to the ultraviolet region of the solar spectrum [9]. Also, the electron mobility of TiO_2 is too low, thus inferior conversion efficiency of solar cells [10,11]. To enhance light harvest in the visible light region, many efforts have been made by focusing on the development of high performance sensitizers [12–15]. It is still a challenge to obtain an ideal organic dye as sensitizer to absorb photons in the full sunlight spectra. For this reason, Semiconductors such as CdS, CdSe, CdTe, PbS, Bi_2S_3, $CuInS_2$, and so on, which absorb light in the visible, can serve as sensitizers because they are able to transfer electrons to large band gap semiconductors such as TiO_2 or ZnO [9]. Among this materials CdS with suitable band gaps and band positions compared with TiO_2 create a long distance charge separated state with electron and holes at sites far from each other and hens is useful for using in DSSC. Different methods were used for deposition of CdS on TiO_2 surface but Chemical method has been demonstrated to be a facile method because of the low cost equipments involved, lower growth temperature and reproducibility. In these work different chemical methods such as microwave (MW), hydrothermal (HT), chemical bath deposition (CBD), successive ionic layer adsorption and reaction (SILAR) and doctor blade (DB) were used for deposition of CdS on the TiO_2 surface and their effects on optical properties and solar cell efficiency were studied. It is well accepted that different methods of preparing semiconductor would lead to solar cells of different overall properties resulting in different efficiencies. Each method has advantages for using in this experimental work: Hydrothermal method would lead to quality improvement, lower costs and environmental friendly processing [16–19]. Also, microwave dielectric heating is rapidly becoming an established procedure in synthetic chemistry [20]. Chemical bath deposition (CBD) is known to be a simple, low temperature, and inexpensive large-area deposition technique. It has been used in the deposition of CdS semiconductor thin films since the 1960s [21]. Also, SILAR has a number of advantages for using in deposition process: (i) it offers extremely easy way to dope film with virtually any element in any proportion by merely adding it in some form of the cationic solution, (ii) unlike closed vapor deposition method, SILAR does not require high

* Corresponding author. Tel.: +98 361 5555 333, fax: +98 361 555 29 30.
E-mail address: salavati@kashanu.ac.ir (M. Salavati-Niasari).

0013-4686/$ – see front matter © 2013 Elsevier Ltd. All rights reserved.
http://dx.doi.org/10.1016/j.electacta.2013.11.176

quality target and/or substrates nor does it require vacuum at any stage, which is a great advantage if the method will be used for industrial application, (iii) the deposition rate and the thickness of the film can be easily controlled over a wide range by changing the deposition cycles, (iv) operating at room temperature can produce films on less robust materials, (v) unlike high power methods such as radio frequency magnetron sputtering (RFMS), it does not cause local over heating that can be detrimental for materials to be deposited and (vi) there are virtually no restrictions on substrate material, dimensions or its surface profile. Moreover, it is relatively inexpensive, simple and convenient for large area deposition [22]. To our knowledge, this is the only successful work to study the effect of deposition method on the optical properties and solar cell efficiency of TiO_2/CdS DSSC.

2. Experimental

2.1. Deposition method

EPD was utilized to the preparation of P25 NPs-based films used in DSSCs. During EPD, the cleaned FTO glass remained at a positive potential (anode) while a pure steel mesh was used as the counter (cathode) electrode. The linear distance between the two electrodes was about 3 cm. Power was supplied by a Megatek Programmable DC Power Supply (MP-3005D). The applied voltage was 10 V. The deposition cycle was 4 and 8 times with each time of 15 s, and the temperature of the electrolyte solution was 25 °C. The coated substrates were air dried. The apparent area of the film was 1×1 cm^2. The resulting layer was annealed under an air flow at 325 °C for 5 min, at 375 °C for 5 min, at 450 °C for 15 min and 500 °C for 15 min °C. Electrolyte solution and the amount of additives are important for creation a surface with high quality. Based on other experiment reported previously [23] we used optimal concentrations of additives in the electrolyte solution as follows: I_2 120 mg/l, acetone 48 ml/l, and water 20 ml/l. A mechanism was proposed by Koura et al. [24] that state the particle charging in this system is achieved via adsorption of protons, which are formed by the keto-enol reaction:

$$CH_3COCH_3 \leftrightarrow CH_3C(OH)CH_2$$

$$CH_3C(OH)CH_2 + I_2 \rightarrow CH_3COCH_2I + H^+ + I^-$$

Scheme 1a shows EPD process. Deposition of CdS via SILAR method was initiated by preparation of two solutions, separately. 60 ml of 0.05 M $Cd(NO_3)_3.4H_2O$ ethanol solution (solution 1) and 60 ml of 0.05 M thioacetamid ethanol solution (solution 2). The TiO_2 electrode was immersed in the solution 1 for 1 min, to allow Cd^{2+} to adsorb onto the TiO_2 surface, and then rinsed with ethanol for 1 min to remove the excess Cd^{2+}. The electrodes were then dried for 2 min in air atmosphere. Subsequently, the dried electrode was dipped in to the solution 2 for 1 min. The electrode was then rinsed in ethanol for 1 min and dried again in air atmosphere. This procedure was repeated several times to get desired CdS loading (Scheme 1b). In order to deposition of CdS on the TiO_2 by CBD method, 30 ml of 0.05 M $Cd(NO_3)_3$.4H2O aqueous solution and 30 ml of 0.05 M thioacetamid aqueous solution were prepared and stirred for 15 min, separately. After that two solutions were mixed together and the final solution was stirred for 15 min and heated to 80 °C. Then the TiO_2 electrode was immersed in the solution for 20 seconds and was air dried. This process was continued for 8 times. A thin yellow layer was deposited on the TiO_2 electrode (Scheme 1c). To deposition of CdS by MW method, CdS solution was prepared similar to CBD solution in a Teflon beaker. Then the TiO_2 electrode was placed in the bottom of beaker and exposed to the microwave irradiation for 3 min (30 second on and 60 second off).

Table 1
The samples preparation conditions.

Sample No	TiO_2 Electrophoresis Cycles	CdS deposition method
1 (S1)	4	----------
2 (S2)	8	----------
3 (S3)	4	SILAR
4 (S4)	4	CBD
5 (S5)	4	MW
6 (S6)	4	HT
7 (S7)	4	DB
8 (S8)	8	SILAR

S7*: TiO_2/CdS composite prepared via hydrothermal method.

Finally CdS layer was created on the TiO_2 surface (Scheme 1d). The solution that was used for deposition by HT method was prepared according to CBD so;ution. The TiO_2 electrode was then inserted in the bottom of beaker and it was placed in the autoclave. The reaction was done in 120 °C for 24 h. After that, a dark yellow thick layer was obtained. TiO_2/CdS nanocomposite was synthesiszed as follow: 100 ml of 0.004 M $Cd(NO_3)_3.4H_2O$ and 0.1 M of and TAA solutions were prepared sperately and then mixed together. 0.18 gr CTAB and 6 ml of Ti were then added into the final solution. The solution was transformed to the autoclave and the reaction was done in 100 °C for 10 h and 140 °C for 72 h. The obtained powdre was washed with ethanol and distilled water for several times and then dired in 80 °C for 24 h in a vacume oven. For deposition of TiO_2/CdS powder on the FTO glass substrate, a paste of nanocpmosite was initially prepared. The slurry was produced by mixing and grinding 1.0 g of the nanometer sized TiO_2/CdS with ethanol and water in several steps. Then, the grinded slurry was sonicated with ultrasonic horn (Sonicator 3000; Bandeline, MS 72, Germany) and then mixed with terpineol and ethyl cellulose as binders. After removing the ethanol and water with a rotary-evaporator, the final paste was prepared. The prepared TiO_2/CdS paste was coated on fluorinated tin oxide glass (FTO glass, Pilkington Glass, TEC7) by a doctor blade technique. after that the electrode was gradually heated under an air flow at 325 °C for 5 min, at 375 °C for 5 min, at 450 °C for 15 min and 500 °C for 15 min °C. Table 1 shows the samples preparation conditions.

2.2. Cell assembly

The fabricated electrodes were separately immersed into a cis-di(thiocyanato)-N,N'-bis(2,20-bipyridyl-4-carboxylic acid-40-tetrabutylammonium carboxylate) ruthenium (II) (N-719) (Dyesol) dye solution in ethanol (0.5 mM) and kept at room temperature for 48 h to complete the sensitizer uptake. The dye-adsorbed TiO_2 electrodes were then rinsed with ethanol and dried under a nitrogen stream. A Pt coated FTO glass electrode was prepared as a counter electrode. The Pt electrode was placed over the dye-adsorbed TiO_2 electrode and the edges of the cell were sealed with 50 lm thick sealing sheet (Surlyn 50, Dyesol). Sealing was accomplished by pressing the two electrodes together on a double hot-plate at a temperature of about 110 °C. The I^{3-}/I^-electrolyte (Dyesol) was introduced into the cell through one of two small holes drilled in the counter electrode. Finally, these two holes were sealed by a small square of sealing sheet. After that DSSCs were characterized by I-V and EIS spectra.

2.3. Materials and methods

The chemical reagents including Tetraethylorthotitanat ($C_8H_{20}O_4Ti$), $Cd(NO_3)_3.4H_2O$, thioacetamide (TAA), used in our experiments were purchased from Merck. Commercially-available TiO_2 powder of P25 (av. 30 nm by Brunauer-Emmett-Teller (BET), 80% anatase (d = 21 nm) and 20% rutile (d = 50 nm) was prepared

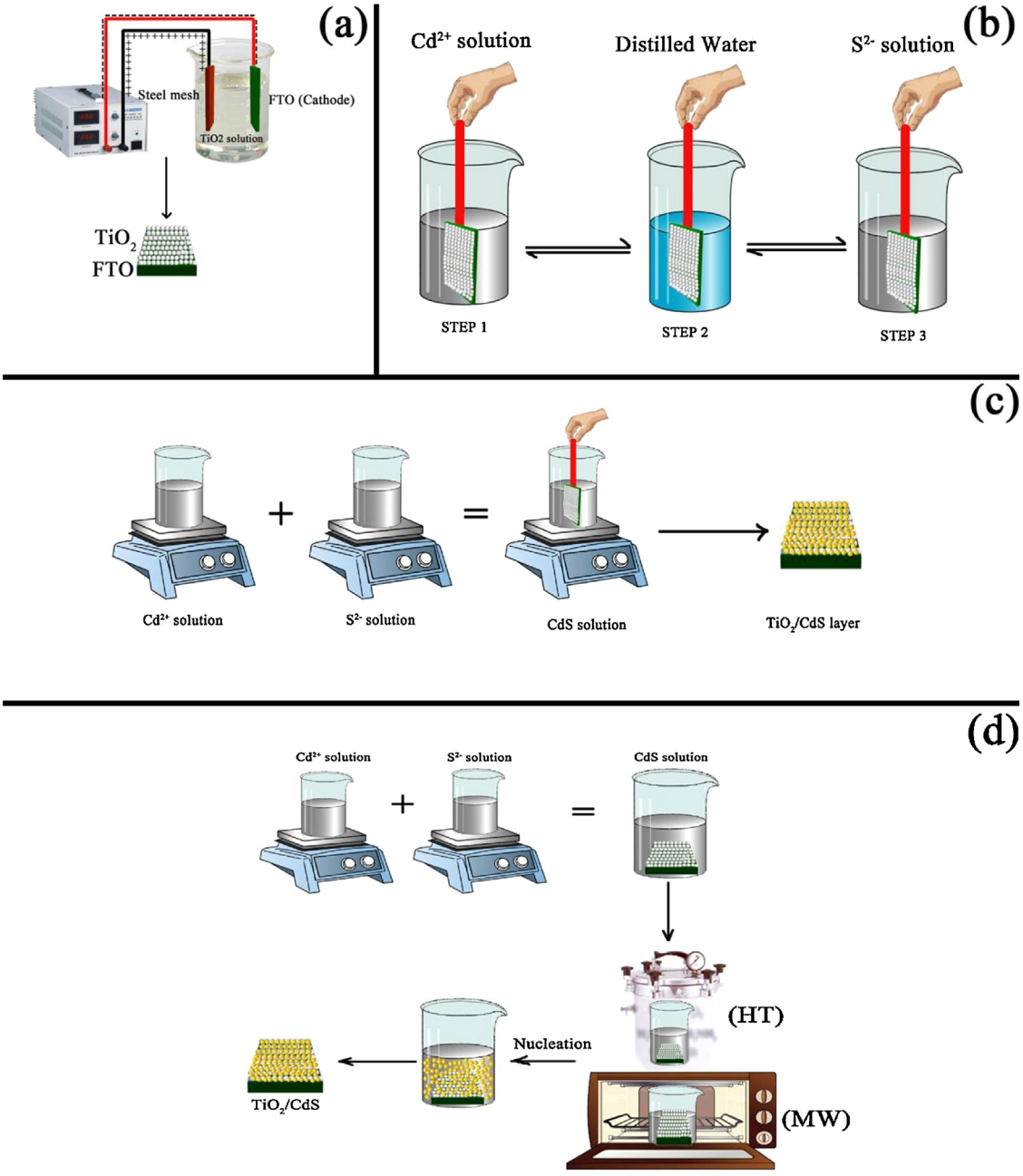

Scheme 1. The samples preparation methods. a) EPD, b) SILAR, c) CBD and d) HT-MW.

from Degussa, Germany. I^{3-}/I^{-} electrolyte, N719, Pt solution, surlyn were purchased from Dyesol. All the mentioned chemicals were used as received without further purification.

For characterization of the products XRD patterns were recorded by a Rigaku D-max C III, X-ray diffractometer using Nifiltered Cu Ka radiation. Atomic force microscopy (AFM) model NT-MDT Solver P47 was used in tapping mode for morphological characterization using ultrasharp Si cantilevers. SEM micrographs were taken by using a field-emission scanning electron microscope (HITACHI S4160, Japan). DRS spectra were recorded using a UV–Vis spectrophotometer (Shimadzu, model UV-3101).The energy dispersive spectrometry (EDS) analysis was studied by XL30, Philips microscope. Transmission electron microscope (TEM) images were obtained on a Philips EM208S transmission electron microscope with an accelerating voltage of 100 kV. Cross-section SEM images were obtained by scanning electron microscope (SEM) (Philips XL- 30ESM). EIS spectra are measured with the electrochemical analyzer (Biologic science instrument, SP-150). Photocurrent density–voltage (J–V) curve was measured by using computerized digital multimeters (Ivium-n-Stat Multichannel potentiostat) and a variable load. A 300 W metal xenon lamp (Luzchem) served as a simulated sun light source, and its light intensity (or radiant power) was adjusted to simulated AM 1.5 radiation at 100 mW/cm^2 with a filters for this purpose.

3. Result and Discussion

3.1. X-ray diffraction pattern

Fig. 1 shows XRD patterns of FTO glass substrate, S1-S6 and S8, respectively. XRD pattern of bare FTO glass (Fig. 1a) shows the diffraction peaks around 2θ= 26.511°, 33.770°, 37.843°, 51.613°,

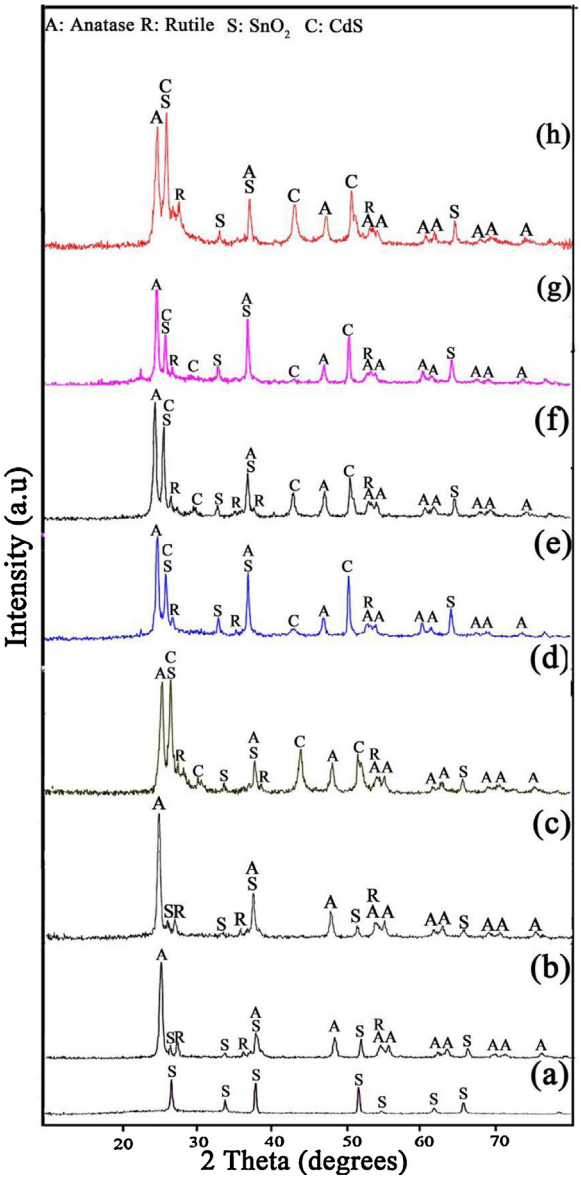

Fig. 1. (a-h). XRD patterns of FTO glass and Samples No 1- 6 and 8, respectively.

54.593°, 61.691°, 65.754°. The characteristic diffraction peaks of S1 and S2 are present in Fig. (1b and 1c). It is well known that the diffraction peaks of TiO_2 nanoparticles (P25 Powder) are consistent with that of anatase and rutile, and anatase is the main phase. Fig. 1d shows XRD pattern of S3. This pattern confirmed that the CdS were successfully formed on the surface of the porous TiO_2 film by SILAR method. Also, CdS was deposited successfully on the TiO_2 film by CBD method (Fig. 1e). In comparison to SILAR method, CBD method was led to create the CdS with lower crystallity that can be attributed to the faster CBD process compared with SILAR method. In fact in the SILAR method the initial materials have enough time to reaction and hence this process is slower than CBD method. XRD pattern of hydrothermal-assisted deposition of CdS on TiO_2 film is depicted in the Fig. 1f. Four kinds of peaks that labeled in this pattern are related to anatase, rutile, FTO and CdS materials. Crystallity level of CdS in this method is the same with the SILAR one. To put it another way, in this method there is enough time for nucleation of CdS on the TiO_2 surface. The XRD pattern of CdS (microwave deposited)/TiO_2/FTO is shown in Fig. 1g. It can be seen that there are CdS peaks with lower crystallity compared with S6.

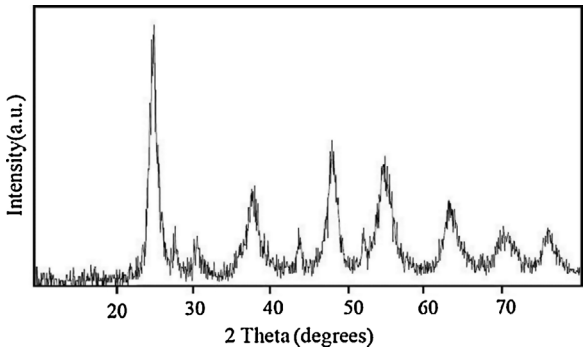

Fig. 2. XRD pattern of S7*.

This is due to higher reaction speed in the microwave approach. So the reagents have not enough time for nucleation process and hence cadmium sulfide with low crystallity will be created. Fig. 1h shows a similar pattern with S3 that indicate the electrophoresis cycles have not important effect on the product structure. The XRD pattern of S7* is present in Fig. 2. It can be seen that TiO_2 structure has two phases (anatase and Orthorhombic). The structure of TiO_2 has a significant role in electron transfer and solar cell efficiency. The best structures of TiO_2 for DSSC are anatase and rutile. Anatase structure is more useful for utilize in DSSC due to follow reasons [25]: 1) electron transfer in anatase is faster than rutile structure due to differences in the extent of interparticle connectivity associated with the particle packing density. 2) also due to smaller surface area per unit volume of the rutile compared with that of the anatase, rutile structure adsorb lower dye molecules on its surface compared with anatase one. so, using chemical methods such as hydrothermal is not led to create a material with expected phases. In fact, despite chemical methods have many advantages for synthesis of materials, but in some cases that needed to creation a material with special features, this kind of methods can't be a good choice. The information of XRD peaks is given in Table 2.

3.2. Energy dispersive X-ray analysis

Fig. 3 (a-c) shows Chemical compositions of the S3-S6 respectively. This figure shows that CdS was successfully coated on the TiO_2 film by each coating methods. Si and Sn peaks are related to the glass substrate.

3.3. SEM images of the surface

The morphology of the fabricated films was investigated by SEM images. Fig. 4 (a-d) shows SEM images of S1, S2, S4 and S3, respectively. TiO_2 film is composed from aggregated particles with a number of cracks in the surface. Based on the work of Jarernboon et al. [26] the TiO_2 surface was comprised of a number of cracks. In Fig. 4a, a crack site is depicted with red rectangular. This crack site was proceed with an image processor software (image j) that shown in the right side. As shown in this figure crack sites act as defect and limit the electron transfer across the electrode that would cause carrier recombination, and subsequently decrease the current density and the energy conversion efficiency. In other words these sites are trap states that catch electrons and prohibit the electron transfer. The chunk-like structures in the surface of TiO_2 electrode is mainly due to aggregation of nanoparticles with high energy for being in form of agglomeration structures. So these two factors (cracks and chunks) restrict the electron transfer to external circuit for creating current. By increasing the TiO_2 film thickness in S2, the cracks and chunks were decreased that can improve electron transfer across the electrode (Fig. 4b). In other words the increase of the

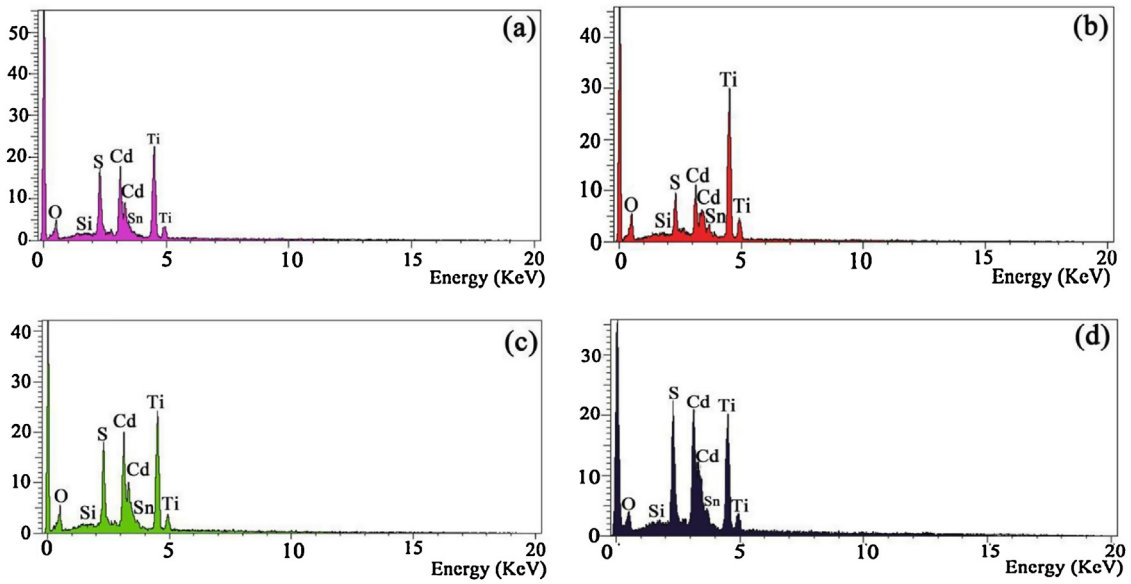

Fig. 3. (a-d). EDS of S3, S4, S5 and S6, respectively.

film thickness can effect on surface quality and electron transfer. Fig. 4c shows SEM image of S4. By using CBD method for deposition of CdS on the TiO_2 surface, the number of cracks will be increased that mainly due to fast cooling of the surface after heating in the solution. The chunk structures in the surface are due three reasons. 1) Different sizes of CdS and TiO_2 nanoparticles, 2) active surface of CdS nanoparticles that lead to aggregation of them on the TiO_2 surface, 3) and finally the exits of chunk structures in the TiO_2 surface. As shown in Fig. 4c (right side), the cracks in the surface are defects that decrease short circuit current density and solar cell efficiency. SEM image of the surface of S3 is shown in Fig. 4d. SILAR method led to creating a surface with more cracks in comparison to CBD method that is mainly due to its more heating and cooling steps. Surface plot of a crack structure shows that this site can easily restricts electron transfer across the electrode. It is important that the mobility always drops by at least 2 orders of magnitude with impurities or defects (traps) [27]. The surface SEM image of S5 is shown in Fig. 5a. As shown in this figure due to high speed of heating and cooling of microwave irradiation for deposition of the CdS, crack sites are larger than other methods. Fig. 5b shows SEM image of S6. It can be seen that by hydrothermal method for deposition of CdS on the TiO_2 surface large cracks will be created. The main reason is long time and high level of deposition in this process. In comparison to the previous deposition process, this surface has more chunk structures that can limit electron transfer. As shown in Fig. 5c by deposition of CdS on TiO_2 (8 cycles) via SILAR method the chunk structures and cracks were increased in comparison with S3 that can restrict electron transfer and solar cell performance. It can be concluded that deposition of CdS on the TiO_2 films with different thicknesses by a similar method are led to creating the electrodes with different surface qualities. Other factors can restrict electron transfer is grain boundaries. When the particle size is decreased the borders among them are increased that act as trap centers and limit the short circuit current. Fig. 6 shows SEM images of S7* with different magnification. From this figure we can see that the product is composed of many batches that each one has many small particles. This means that hydrothermal method can lead to creation of the product with tiny particles. Fig. 7 shows a schematic of surface grain boundaries that obtained from SEM images. It can be seen that these sits can trap electrons and restrict solar cell performance.

Table 2
The information of XRD peaks related to Fig. 1 and Fig. 2.

Figure	material	JCPDS	Crystal system	Position (2θ)	Miller indices
1a	SnO_2 (FTO)	01-077-0451	Tetragonal	26.511 - 33.770 - 37.843 - 51.613- 54.593- 61.691- 65.754	(1 1 0), (1 0 1),(2 0 0)- (2 1 1), (2 2 0)- (3 1 0)- (3 0 1)
1b	TiO_2 (anatase)	01-073-1764	Tetragonal	25.367- 37.053- 37.909 - 48.158- 54.051- 55.204- 62.280- 62.867- 68.976- 70.479	(1 0 1)- (1 0 3)- (0 0 4)- (2 0 0)- (1 0 5)- (2 1 1)- (2 1 3)- (2 0 4)- (1 1 6)- (2 2 0)
1b	TiO2 (Rutile)	01-077-0441	Tetragonal	27.387- 36.007- 54.213	(1 1 0)- (1 0 1)- (2 1 1)
1c	TiO_2 (anatase)	01-073-1764	Tetragonal	25.367- 37.053- 37.909 - 48.158- 54.051- 55.204- 62.280- 62.867- 68.976- 70.479	(1 0 1)- (1 0 3)- (0 0 4)- (2 0 0)- (1 0 5)- (2 1 1)- (2 1 3)- (2 0 4)- (1 1 6)- (2 2 0)
1c	TiO2 (Rutile)	01-077-0441	Tetragonal	27.387- 36.007- 54.213	(1 1 0)- (1 0 1)- (2 1 1)
1d	CdS	01-075-1546	Cubic	26.505- 30.699- 43.969- 52.076-	(1 1 1)- (2 0 0)- (2 2 0)- (3 1 1)
1e	CdS	00-001-0647	Cubic	26.507- 43.917- 51.911	(1 1 1)- (2 2 0)- (3 1 1)
1f	CdS	01-075-1546	Cubic	26.505- 30.699- 43.969- 52.076	(1 1 1)- (2 0 0)- (2 2 0)- (3 1 1)
1 g	CdS	01-075-1546	Cubic	26.505- 43.969- 52.076- 54.579	(1 1 1)- (2 2 0)- (3 1 1)- (2 2 2)
1 h	CdS	01-075-1546	Cubic	26.507- 43.917- 51.911	(1 1 1)- (2 2 0)- (3 1 1)
2	TiO_2 (Anatase)	00-004-0477	Tetragonal	25.354- 37.785- 48.077- 62.728	(1 0 1)- (0 0 4)- (2 0 0)- (2 0 4)
2	TiO_2	01-084-1750	Orthorhombic	25.443- 31.382- 41.839	(1 1 0)-(1 1 1)- (1 0 2)
2	CdS	00-001-0783	Hexagonal	26.668- 28.401-43.917-48.104-52.230	(0 0 2), (1 0 1), (1 1 0), (1 0 3), (1 1 2)

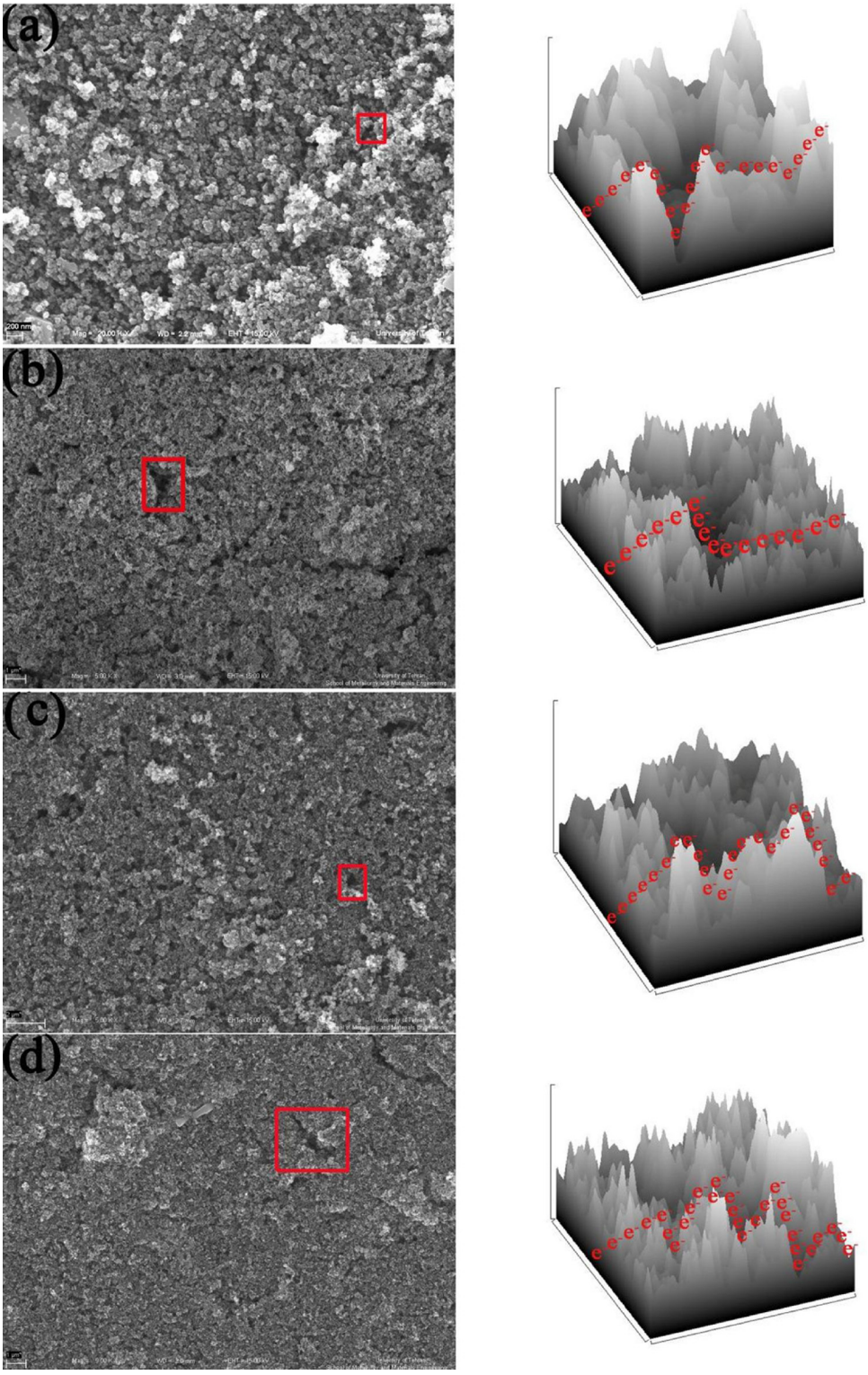

Fig. 4. (a-d). SEM images (left) and 3D crack plots (right) of S1, S2, S4 and S3, respectively.

3.4. Transmission electron microscopy

Fig. 8 shows TEM image of S7*. It can be clearly seen that the sample is mainly composed from very small particles about 2-3 nm that it is in agreement with SEM observation. In fact the product has been composed from clusters of very small particles.

3.5. Histogram of samples particle size

The histogram of particles size distribution from SEM images is shown in Fig. 9. It can be observed that different methods for deposition of CdS on the TiO_2 surface lead to creation of samples with different sizes. Also the films with different thicknesses

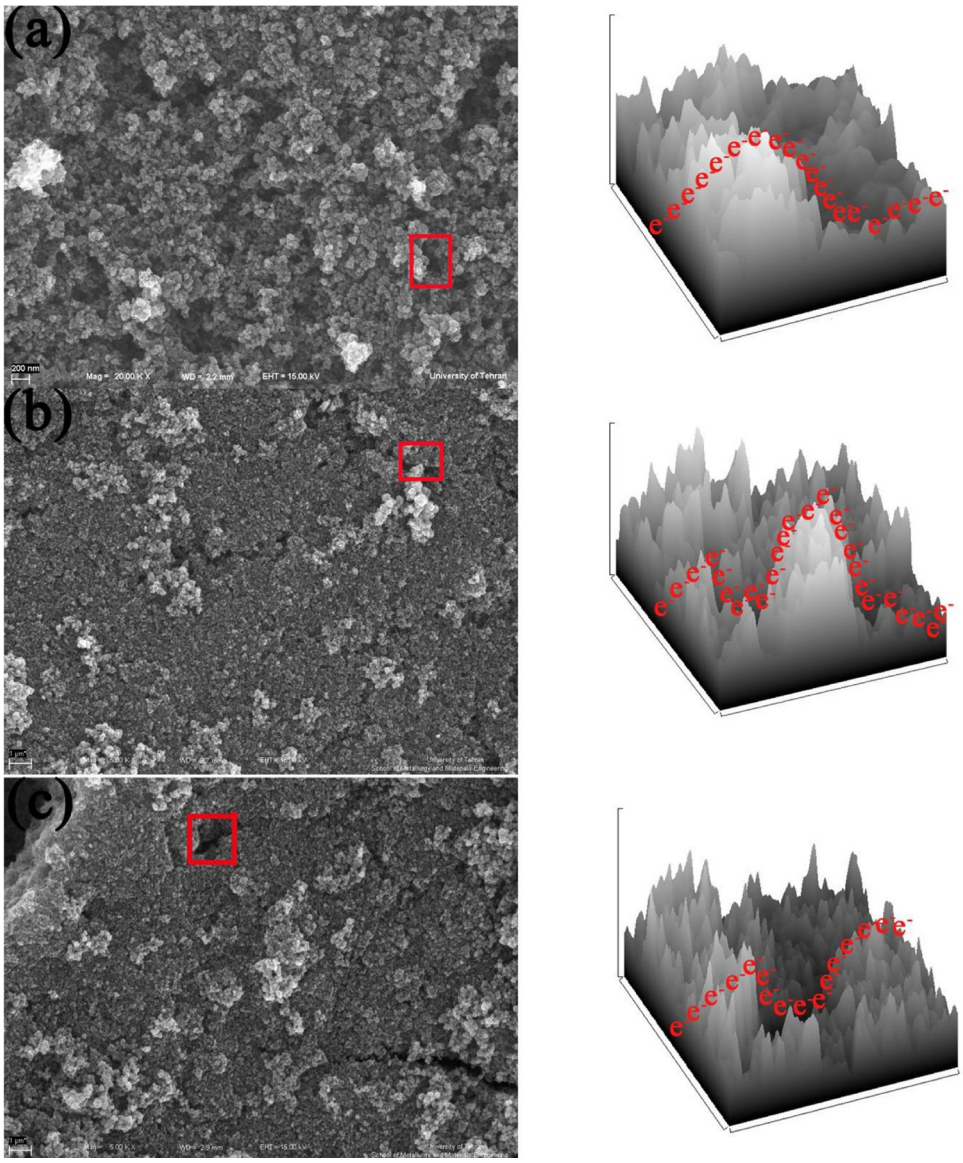

Fig. 5. (a-c). SEM images (left) and 3D crack plots (right) of S5, S6 and S8, respectively.

have different particle sizes in their surfaces. As shown in this figure MW method was led to creating a surface with the smallest particles that can be attributed to high energy value of this method for synthesis of the materials. The largest particles among four deposition methods have been obtained via SILAR method.

3.6. Cross-section SEM images

Fig. 10 (a,b) shows the SEM micrographs of cross-section of the P25 NPs electrode which reveals the thickness of the fabricated P25 electrodes with 4 and 8 cycles electrophoresis has

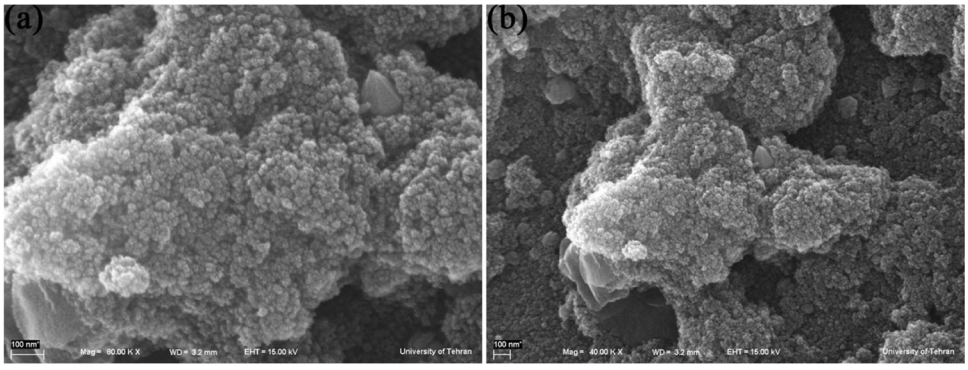

Fig. 6. SEM image of S7* with a) 80 KX and b) 40 KX magnification.

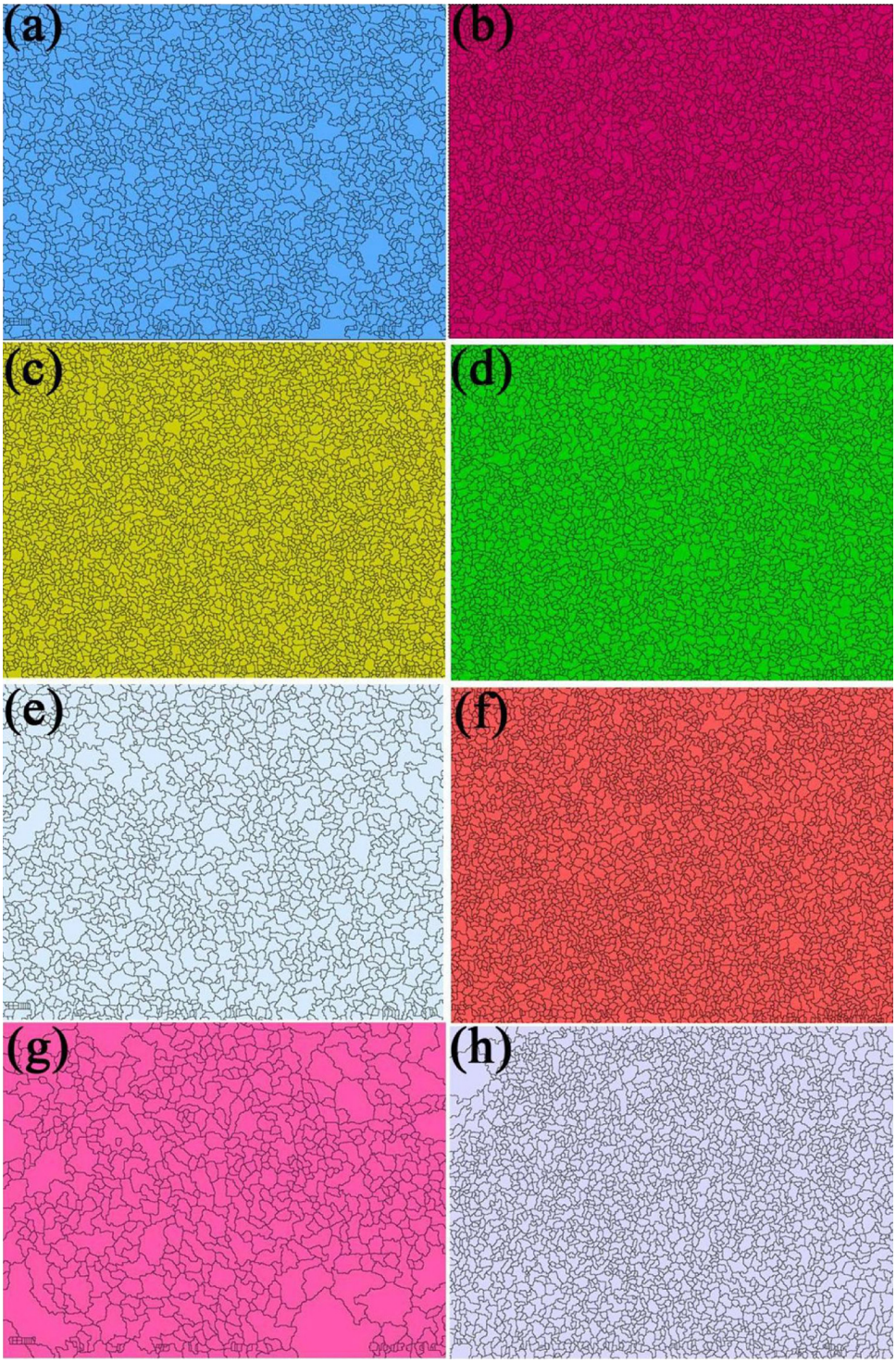

Fig. 7. (a-h). Schematic of grain boundaries of S1- S6, S7* and S8, respectively obtained from SEM images.

4.55 μm and 9 μm, respectively. Since the electrode with thickness of 9 μm prepared the higher efficiency than 4.55 μm electrode and furthermore by increasing the thickness short circuit current density will be decreased, we used TiO_2 electrode prepared by 4 cycles (4.55 μm) as initial electrode for subsequent deposition process. Figure 10 (c,d) shows SEM cross-section of TiO_2/CdS deposited by SILAR and CBD methods, respectively. It can be seen that two electrodes have same thickness that is due to their short time deposition process. When the microwave and hydrothermal methods were chose for deposition process, electrodes with the thickness about 12.38 μm and 22.7 μm were created, separately. This is because of long time of hydrothermal process and hence the amount of deposited CdS on the TiO_2 is increased. Fig. 10g shows SEM cross section of TiO_2/CdS nanocomposite that deposited on the FTO substrate by doctor blade technique. The thickness of the electrode (12.27 μm) shows that control of the thickness with electrophoresis method is better than doctor blade technique. As shown in Fig. 10h, SILAR method was led to deposition a thin layer of CdS on TiO_2 (8 cycles) surface (S8) that can be attributed to its short time deposition process as mentioned earlier.

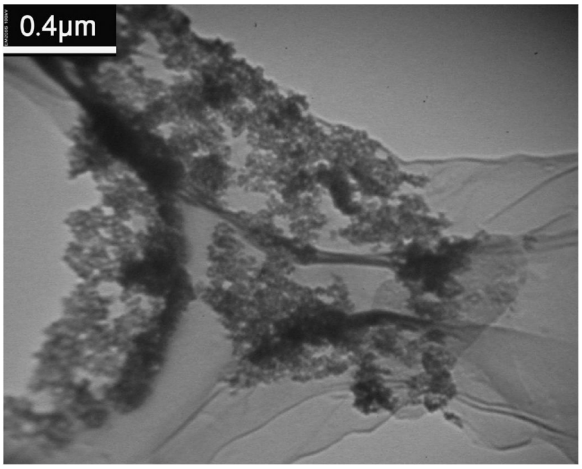

Fig. 8. TEM image of S7*.

3.7. Atomic force microscopy

Fig. 11 (a-c) shows 2D and 3D atomic force microscopy (AFM) images of S1, S3 and S5, respectively. It can be seen that bare TiO_2 electrode shows the uniform surface (Fig. 11a). Also its porosity is high that can improve the dye absorption on the surface and subsequently increase the solar cell efficiency. SILAR method was led to create a surface with lower porosity and bigger crystal size in comparison with bare TiO_2 electrode (Fig. 11b). This can limit the dye absorption and hence restricts the solar cell efficiency. Fig. 11c shows AFM image of CdS/TiO_2 electrode that was prepared by microwave technique. This surface shows irregular structure that can be due to fast and uncontrollable process of microwave method for deposition of CdS on the TiO_2 surface. Also it has the lowest porosity that limits active surface area for dye absorption and therefore decreases the electron transfer from dye molecules to the TiO_2 surface. So it can be concluded that deposition method is a significant factor for determine of porosity level of the surface and hence it influences directly on the solar cell efficiency.

3.8. UV-Vis Diffuse Reflectance spectroscopy

The UV-Vis Diffuse Reflectance spectroscopy of S1, TiO_2/dye, S2, S3 and S4 are shown in Fig. 12 (a-e), respectively. As shown in this figure the shape and position of absorption edges are various. In comparison to the bare TiO_2 electrode (Fig. 12a) the absorption edge of other the electrodes shift to red region. This shift increases visible light absorption and hence is useful for solar cell application. The fundamental absorption edge in most semiconductors follows the exponential law. Using the absorption data the band gap was estimated by Tauc's relationship:

$$(\alpha h\nu) = B\,(h\nu - E_g)^m$$

Where B is characteristic disorder parameter and m depends on the type of electronic transition and can be any value between 0.5 and 3 [28]. For direct transition between valance band and conduction band m = 0.5. A rapid rise in absorption coefficient (α) near the fundamental absorption edge indicates direct energy transition in the forbidden gap. The energy band gap of the samples has been estimated by extrapolating the linear portion of the plots of $(\alpha h\nu)^2$ against $h\nu$ to the energy axis (inset in Fig. 12). The samples show different band gap compared with the TiO_2 bare film. It is obviously that by loading the dye on the TiO_2 surface, due

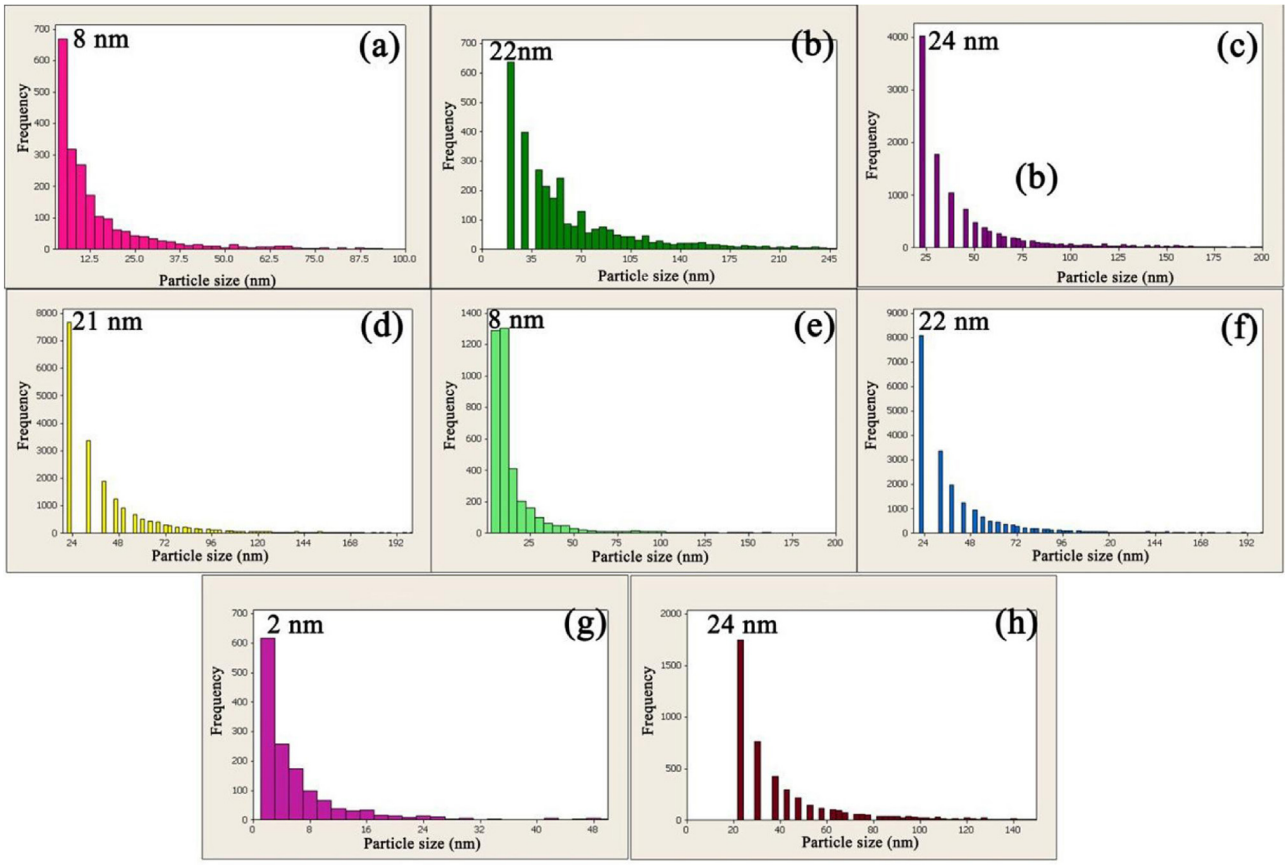

Fig. 9. (a-h). Histogram of particle size of S1-S6, S7* and S8, respectively.

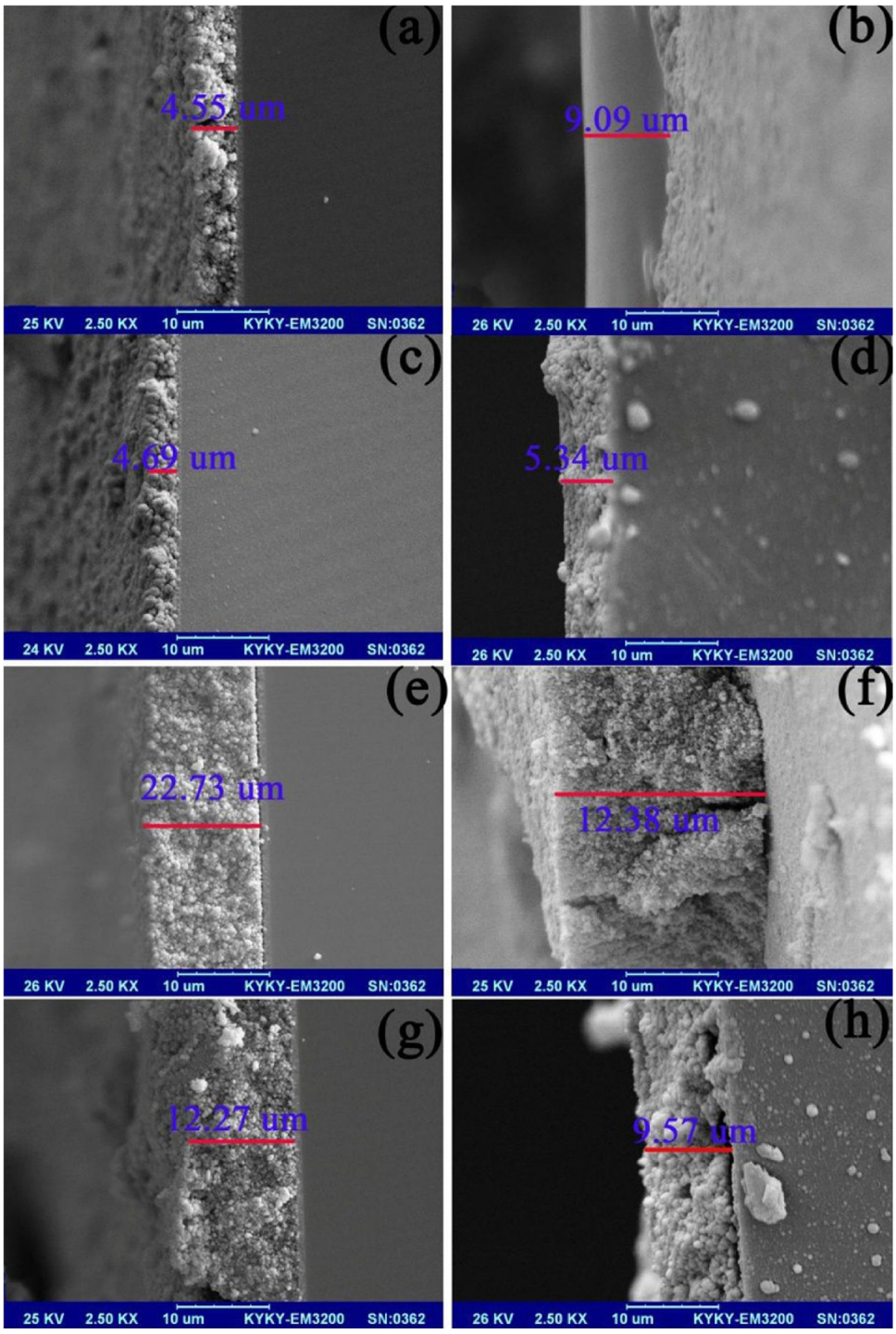

Fig. 10. (a-h). Cross-section SEM images of S1-S8, respectively.

to visible light absorption by dye molecules (E_g= 1.5 eV) the band gap was decreased. Also it can be seen that deposition method is main reason for different samples band gap. In other words different methods for deposition process are led to fabrication a surface with different thicknesses that influence on the optical properties. The absorption coefficient (α) signifies inter-band transition near the band gap and has been calculated using [29]

$$\propto = \frac{1}{t}\ln\left[\frac{(1-R)^2}{2T} + \left(\frac{(1-R)^4}{4T^2} + R^2\right)^{1/2}\right]$$

Where t, T, and R are film thickness, transmittance, and reflectance, respectively. The value of α decrease with increase in thickness of the films and subsequently the value of E_g decreases [30]. In fact, by decreasing the film thickness a blue shift will be appeared in the DRS spectrum that has already been observed in the literature [31,32]. Table 3 shows the band gap of the samples versus their thicknesses. It can be seen that by increasing the thickness the band gap has been decreased. As shown in Fig. 12b, by increasing TiO_2 film thicknesses the band gap will be decreased that is more useful for using in solar cell application in comparison in S1. Fig. 13 (a-d) shows UV-Vis spectroscopy and plot of $(\alpha h\nu)^2$

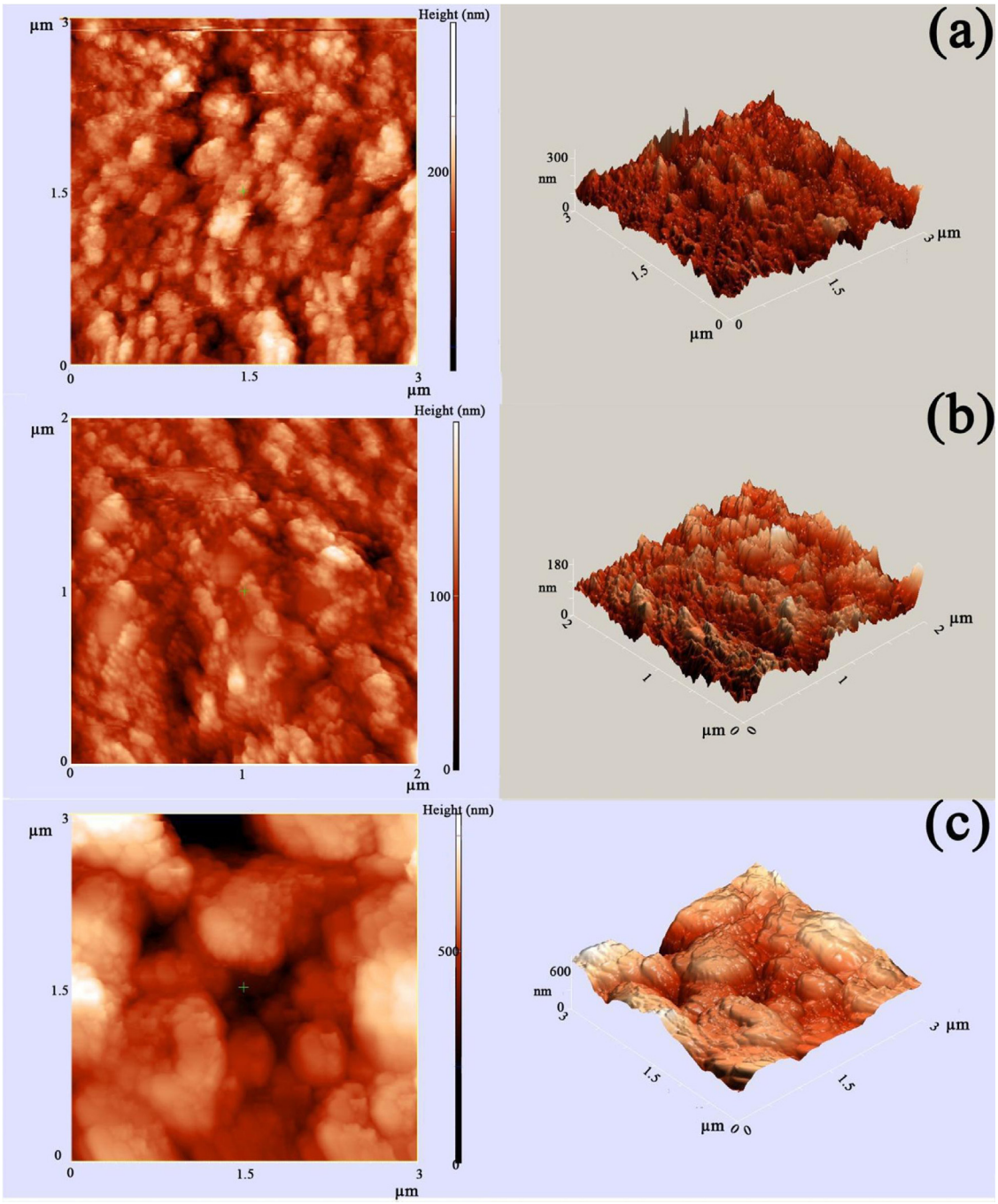

Fig. 11. (a-c). 2D (left) and 3D (right) AFM images of S1, S3 and S5 respectively.

Table 3
The samples band gap, thickness and DSSC performance made by different samples.

Sample No	Band gap (eV)	Thickness (µm)	V_{oc}	I_{sc}	FF	Efficiency (%)
S1	3.1	4.55	0.59	7.817	0.53	2.43
S2	3.0	9.09	0.65	13.37	0.51	4.45
S3	2.4	4.69	0.63	9.16	0.55	3.21
S4	2.3	5.34	0.55	6.61	0.56	2.04
S5	2.2	12.38	0.51	5.7	0.53	1.54
S6	2.09	22.73	0.47	4.42	0.43	0.9
S7	2.9	12.27	0.62	4.04	0.57	1.42
S8	2.1	9.57	0.67	15.43	0.46	4.50

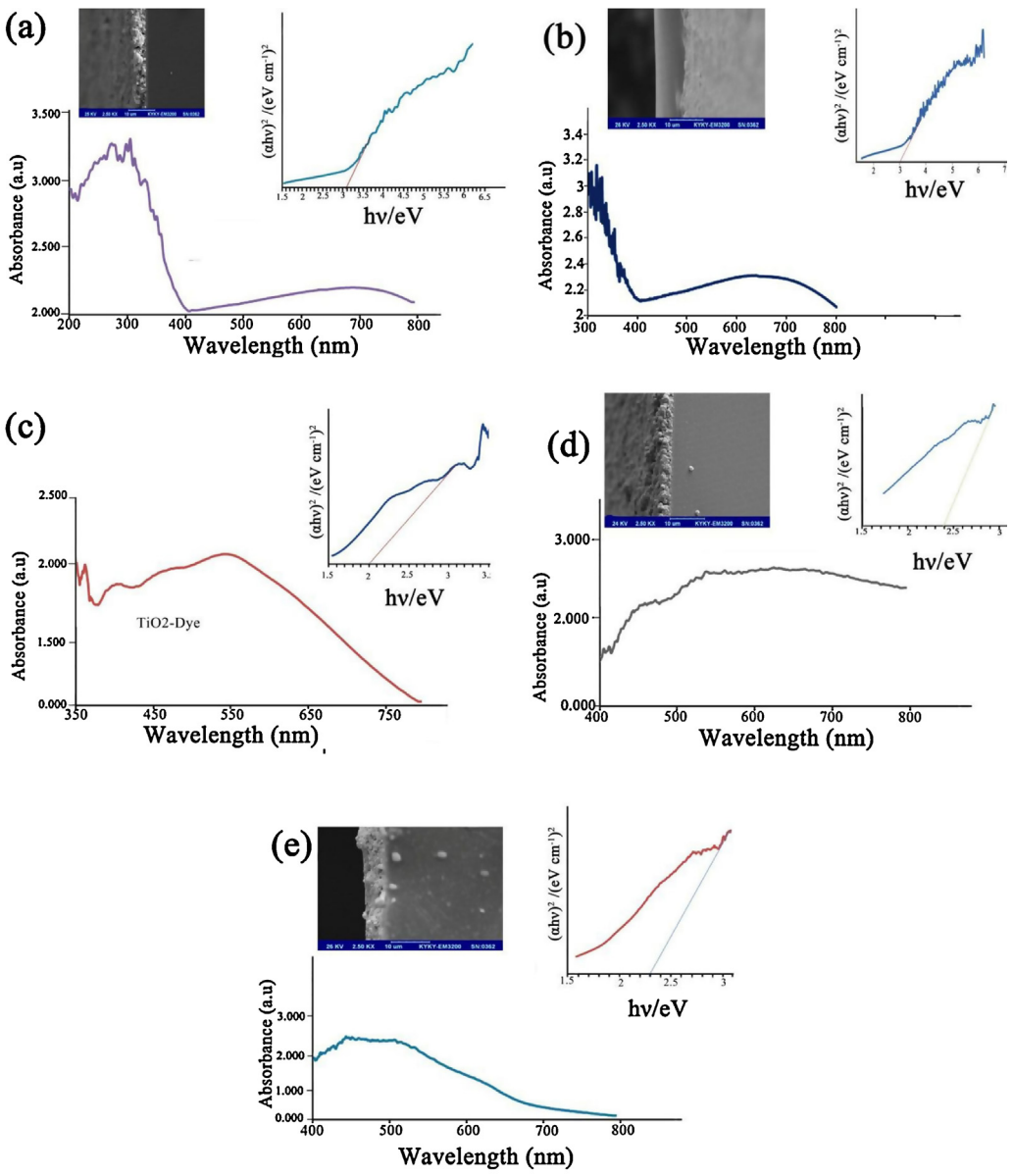

Fig. 12. (a-e). DRS and plot of $(\alpha h\nu)^2$ versus $(h\nu)$ of S1, S2, TiO_2/Dye, S3 and S4, respectively.

versus $(h\nu)$ of the S5-S8. It can be observed that due to the highest thickness related to S6 (Fig. 13b), it has the lowest band gap among the S3, S4 and S5 surfaces. As shown in Fig. 13c CdS was led to shift the band gap of TiO_2 from 3.2 eV to 2.9 eV that can be appropriate factor for increasing the absorption of visible light range. Also by deposition of CdS on TiO_2 (8 cycles) and increase the film thickness the band gap become lower than S3 (Fig. 13d) that shows using this sample is better for solar cell application.

3.9. Cyclic voltammetry

Cyclic voltammetry measurements were done in a standard three-electrode cell using a Ag/AgCl (in aqueous KCl 3 M) reference electrode and a Pt counter electrode. The electrolyte was prepared from aqueous H_2SO_4 solution with pH = 3. Furthermore scan rate 50 mVs^{-1} was selected. Fig. 14 (a-e) shows cyclic voltammetry of bare FTO glass, S1, S2, S3 and S8 respectively. As shown in this figure when TiO_2 was deposited on the FTO glass, a gradual increase in the anodic current at TiO_2 film was observed (Fig. 14b). When TiO_2 was deposited on FTO glass in 8 cycles (Fig. 14 c) the anodic current was increased that indicate this electrode is more practical in solar cell device. Also deposition of CdS on the top of TiO_2 surfaces (4 cycles and 8 cycles) by SILAR method was led to increasing the anodic current (Fig. 14d,e). In fact this method can create the electrode with higher current anodic current. The other cyclic voltammetry spectra which are depicted in Fig. 15 show that other methods can't increase the anodic current of TiO_2. It can be seen that these methods decrease the anodic current of TiO_2 film in a magnitude value.

3.10. Dye adsorption value

For evaluation the amount of dye adsorption on the surface of electrodes, an alkaline solution from dissolving of 0.05 gr NaOH in 100 ml distilled water was prepared and the electrodes were then placed into 10 ml of the solution for 24 h separately. After that the desorbed dye solution were characterized by UV-Vis spectroscopy. The results are given in the Fig. 16. Higher absorbance

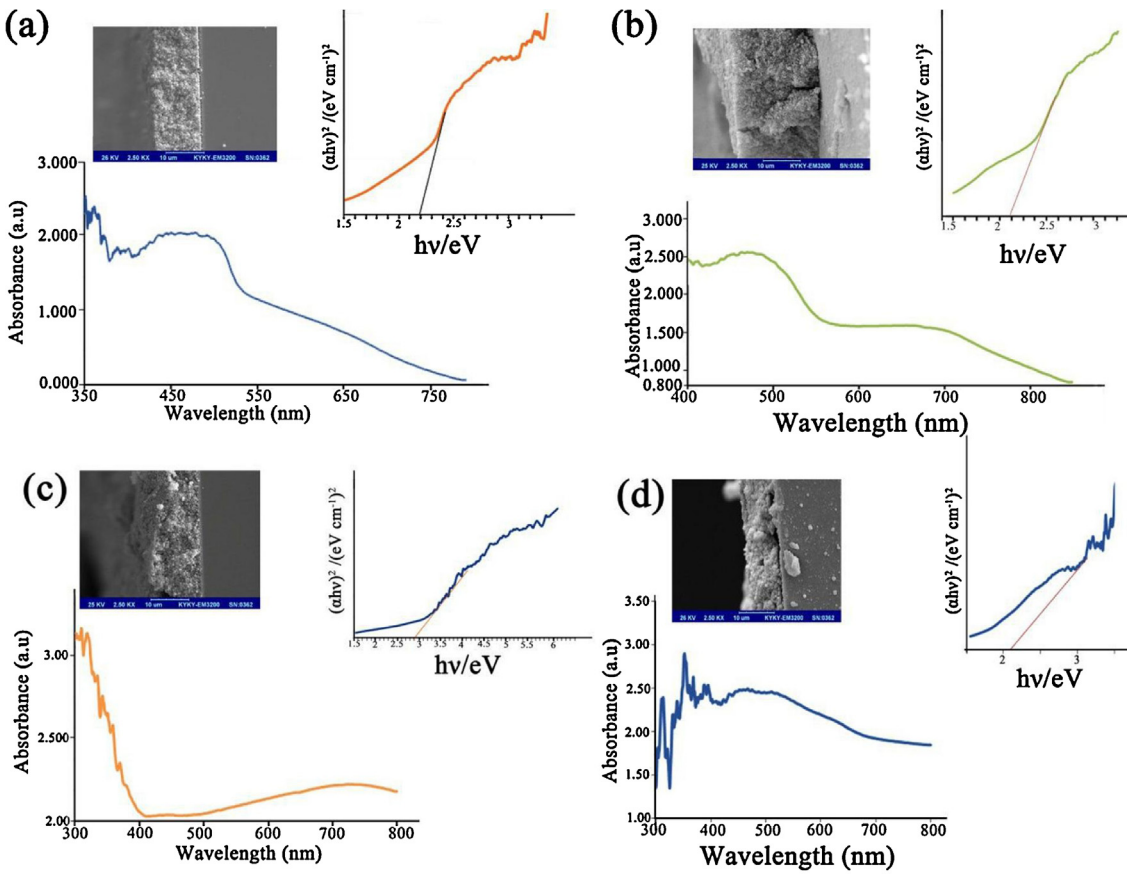

Fig. 13. (a-d). DRS and plot of $(\alpha h\nu)^2$ versus $(h\nu)$ of S5-S8, respectively.

coefficient in the spectra shows higher dye adsorption on the electrode. As shown in this figure, TiO_2 film thickness has important role in dye adsorption value and by increasing the thickness the dye adsorption will be increased. So in this experimental work bare TiO_2 electrode that made by 8 cycles electrophoresis process (S2) shows the maximum dye adsorption and by deposition of CdS on the surface this value will be decreased. This indicates that deposition of CdS on the TiO_2 surface decrease the active surface area and porosity which are important factors for dye adsorption. The amount of dye adsorption dependents to the surface porosity and thickness that by increasing these factors dye adsorption value will be enhanced. For comparison among the surfaces made by SILAR, CBD, MW and HT methods the SEM images of their surface were proceed with an image processing and the plot of the surfaces were obtained (Fig. 17). From this figure, it can be found that the S1 and S2 have the highest porosity and they can adsorb more dye molecules rather than other samples. Among the CdS/TiO_2 surfaces the sequence of the porosity value of the films is S8, S3, S4, S5 and S6, respectively. Furthermore it was found that the surfaces made by SILAR and CBD methods adsorbed dye molecules more than the MW and the HT methods which can be said the porosity of the surface is a dominant factor for dye adsorption. The electrode made by doctor bald from TiO_2/CdS composite shows the lowest adsorption dyes that can be attributed to the lower porosity of its surface due to very small particles and dense structure. Other reason that restricts dye adsorption for TiO_2/CdS composite is existent of TiO_2 with Orthorhombic phase that can't adsorb dye molecules similar to anatase structure.

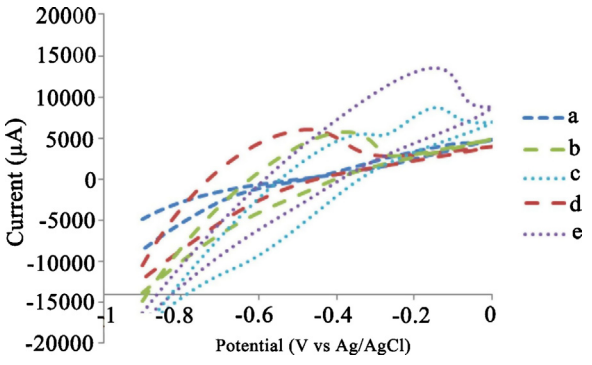

Fig. 14. (a-e). Cyclic Voltammetry (CV) of FTO glass, S1, S2, S3 and S8 respectively.

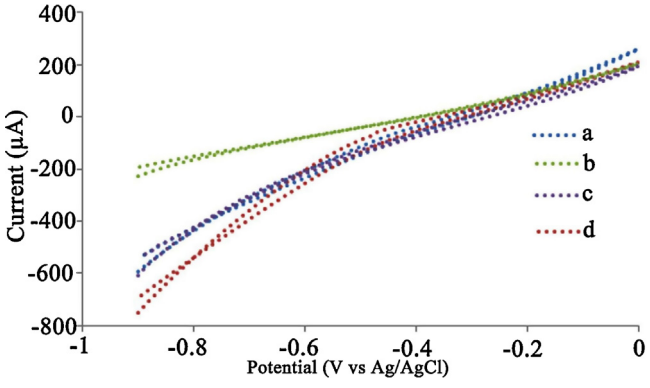

Fig. 15. (a-d). Cyclic Voltammetry (CV) of S4, S5, S6 and S7, respectively.

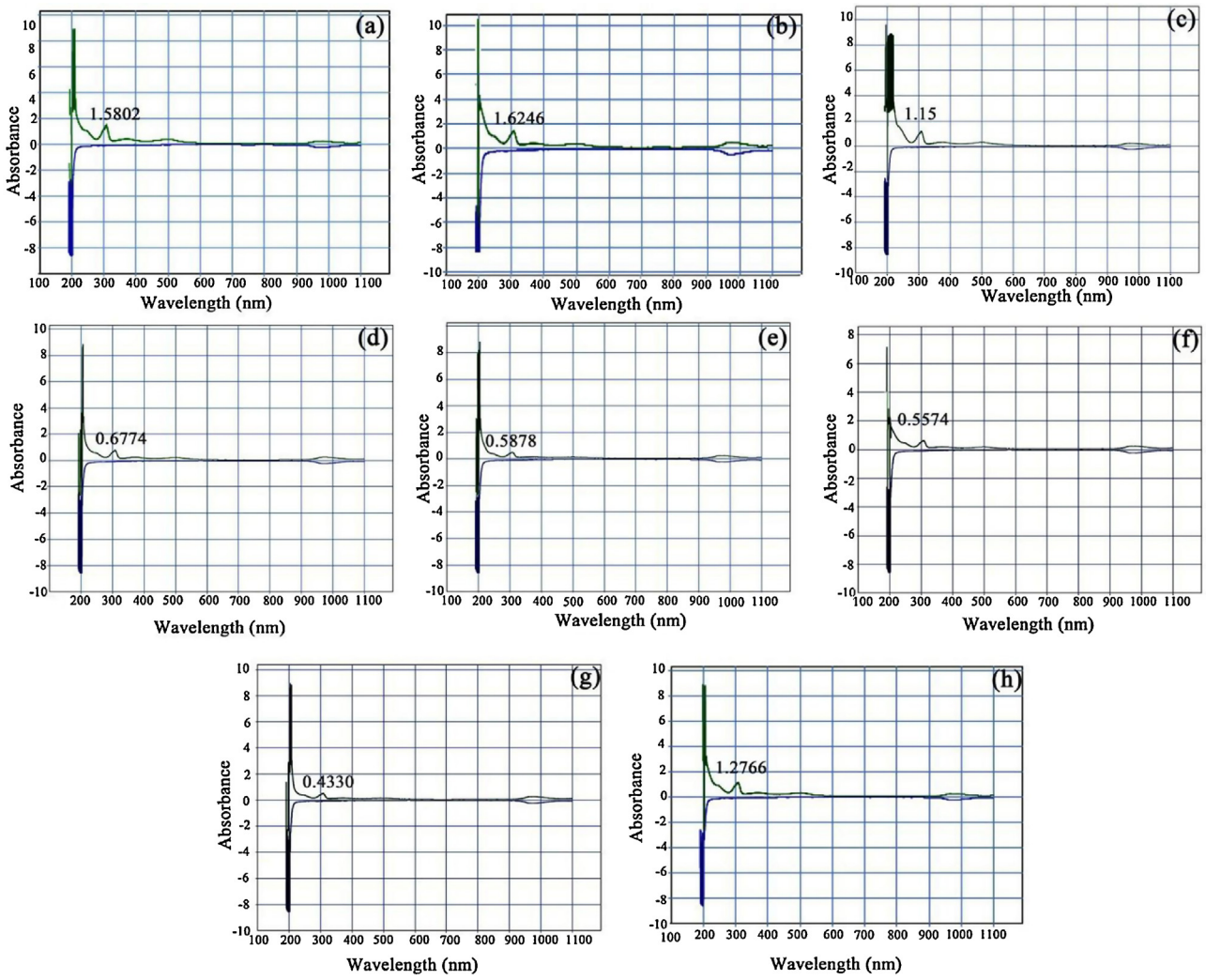

Fig. 16. (a-h). UV-Vis of dye solution desorbed from S1-S8 surfaces respectively.

3.11. IV characteristics

For having a comparison between performances of DSSCs fabricated from different samples, current density–voltage (J–V) curves were obtained (Fig. 18). It is clear that the DSSC performance extremely depends on the TiO_2 film thickness because changing the film thickness changes A_{dye}, J_{sc}, and, η owing to the change of total TiO_2 surface area [33,34]. It is observed that J_{sc} and V_{oc} of the bare TiO_2 electrode with low thickness (S1) are lower than S2. The difference in photocurrent and voltage is found to be related to the lower surface area of S1 compared with S2. In fact by increasing the thickness of TiO_2, dye loading will be increased and followed by increasing the electron-hole creation. FF and efficiency are also increased by increasing the thickness and therefore S2 shows better performance in solar cell. It can be seen that using SILAR method was led to increasing the V_{oc} and J_{sc} of the solar cell. In fact electron transfer from dye molecules becomes more facile by using CdS. FF and efficiency of DSSC is improved by CdS too. Although TiO_2/CdS surface has lower porosity and dye absorption compared with bare-TiO_2 surface, but due to its conduction band position (schematic 2) electron transfer from dye to TiO_2 becomes easier and the number of electrons that can transfer to the external circuit will be increased. Other methods for deposition of CdS on the TiO_2 surface are not appropriate for improving photocurrent and voltage of DSSC. In fact there are many reasons for this such as low porosity, high thickness and more crack sites on the surfaces compared with the bare TiO_2 electrode. Low porosity of the surface will be led to decrease dye loading and hence J_{sc} will be dropped. High thickness and crack sites decrease the open circuit voltage. This is explained as a consequence of the higher charge recombination and restricted mass transport in thicker films due to the augmentation of surface area [35–37]. S 4, S5 and S6 have different porosity and dye loading and hence they have difference short circuit current. Also their thicknesses are various and this affect on recombination sites number and therefore their open circuit voltage are various. S7 has the minimum porosity and dye absorption so it has the lowest J_{sc} compared with other samples. In addition due to TiO_2 has orthorhombic phase and it was not useful for DSSC the dye adsorption on S7 surface and J_{sc} have been decreased. Its V_{oc} is higher than S4, S5 and S6 that it can be concluded the film has lower trap states and hence recombination centers will be decreased. In an extra experiment, SILAR method was served for deposition of CdS on the TiO_2 surface with 9 μm in thickness to investigation of its performance in DSSC. Using S8 for solar cell application was led to better performance related to S3 that can be attributed to the higher dye adsorption and the higher thickness of S8 related to S3. Furthermore, it was found that this method can improve entire solar cell parameters of S2. In other words SILAR method is useful for increasing solar

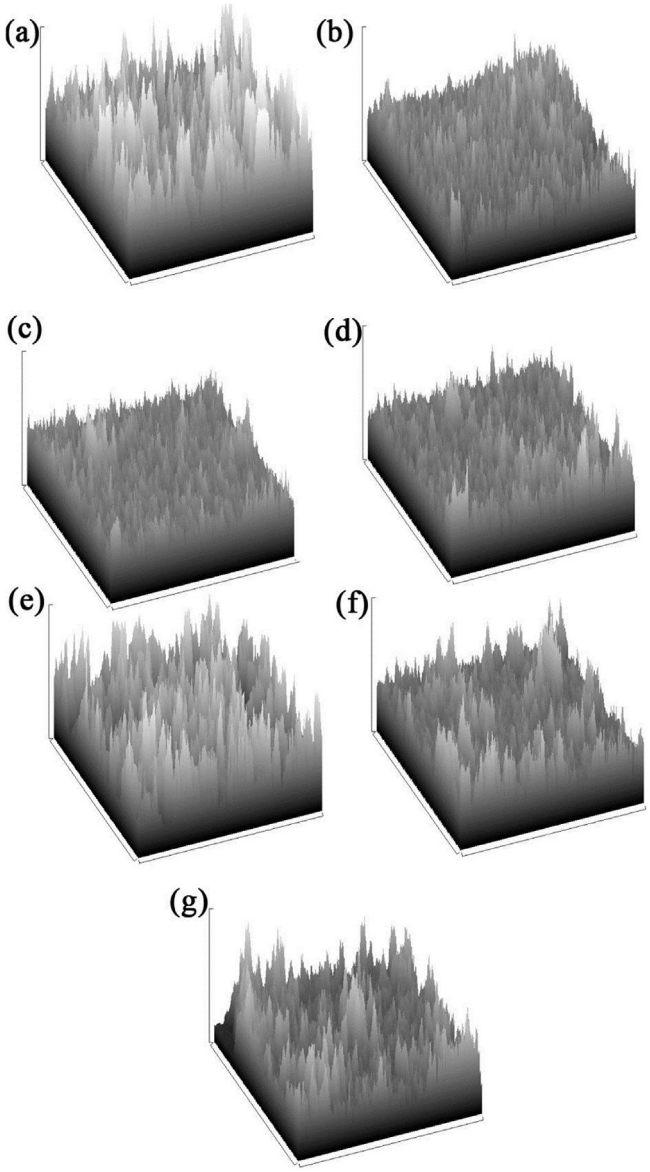

Fig. 17. (a-g). Plot surface of SEM images of S1-S6 and S8, respectively.

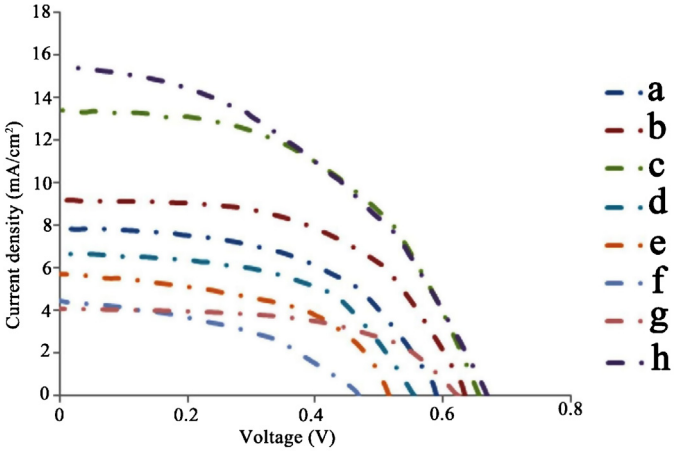

Fig. 18. (a-h). J-V curves of solar cells with the electrodes of S1-S8, respectively.

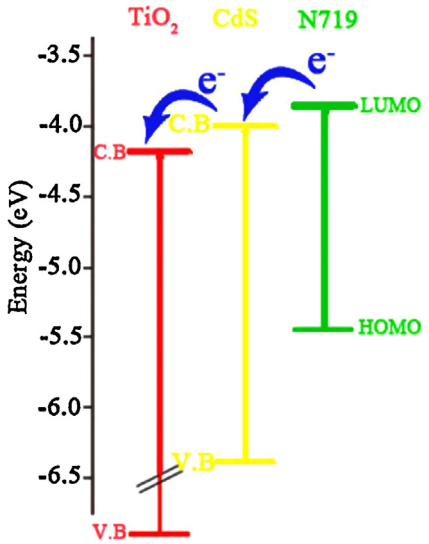

Scheme 2. Schematic energy diagram of HOMO and LUMO for N719 dye, compared to the energy levels for TiO_2 and CdS.

cell efficiency for both 4.55 μm and 9 μm. Fig. 19 shows diagram of different solar cell parameters of the samples. As shown in this figure, it can be said that different methods for deposition of CdS play key role to solar cell performance. In fact different methods fabricate the films with different features such as porosity, dye loading, thickness and cracks that entire of them can influence on efficiency of the DSSCs. Table 3 shows samples band gap and thickness and their solar cell features (Scheme 2).

3.12. EIS spectra

Fig. 20 shows EIS spectra of related to DSSCs that were fabricated by S1, S2, S3 and S8 electrodes respectively. There are usually two or three arcs or semicircles in the Nyquist diagram of DSSC. The first, second and third semi-circles correspond to the charge-transfer resistances at the counter electrode, at the TiO_2/dye/electrolyte interface, and to the Warburg diffusion process of I^-/I^{3-} in the electrolyte, respectively [38]. Here it has just shown the second semicircles. It was found that by increasing the TiO_2 film thickness the resistance of TiO_2/dye/electrolyte interface was decreased that can be attributed to enhance of dye adsorption in thicker film (Fig. 20a). In other words by increasing the dye adsorption by thicker film electron transfer becomes easier and the resistance will be decreased. Also it can be seen that deposition of CdS on the TiO_2 surface has been led to decrease the resistance of TiO_2/dye/electrolyte interface (Fig. 20b). This induces the reduction of the total internal resistance and the improvement of the cell efficiency. This means that electron transfer will be increased by deposition of CdS on the TiO_2 surface. In comparison to S3, sample No.8 (S8) shows the lower resistance that can be due to the higher dye adsorption by S8 as mentioned earlier. Schematic presents an energy-level diagram related to TiO_2, CdS and N719 dye molecules. From this diagram, it can be seen that the bottom of the CB of CdS (CB; −3.98 eV) and the top of the valence band (VB; −6.38 eV) [39] are lower than the LUMO of the dye (−3.8 eV) and the highest occupied molecular orbital (HOMO; −5.4 eV) energy levels, and are also higher than the CB (−4.2 eV) and VB (−7.4 eV) of TiO_2, respectively. It can be seen that the photogenerated electrons in the dye molecules with a high kinetic energy can readily tunnel through the CdS layer and inject into the TiO_2 electrode.

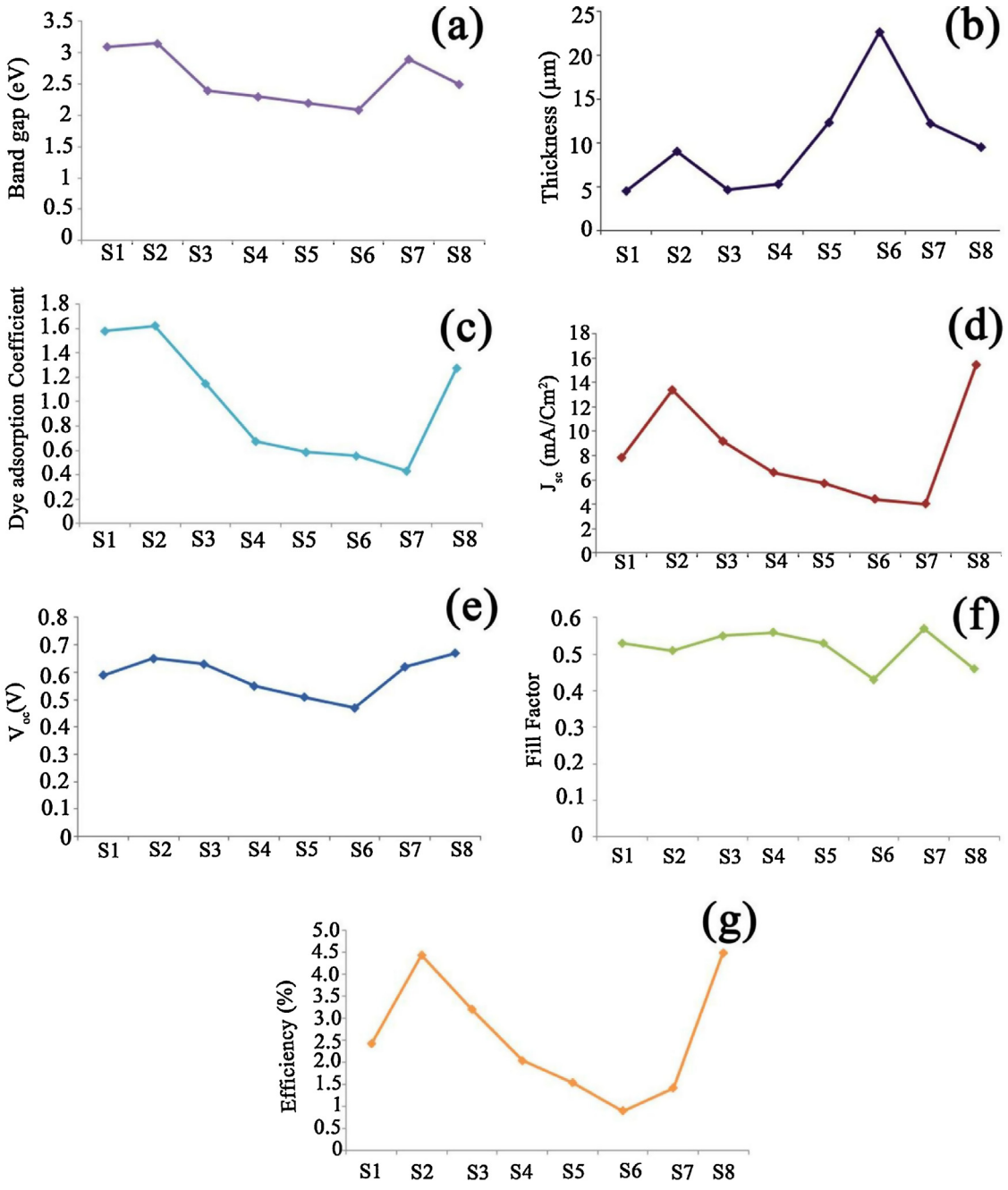

Fig. 19. Diagram of a) band gap, b) thickness c) dye adsorption coefficient d) J_{sc}, e) V_{oc}, f) fill factor and g) efficiency versus the sample number.

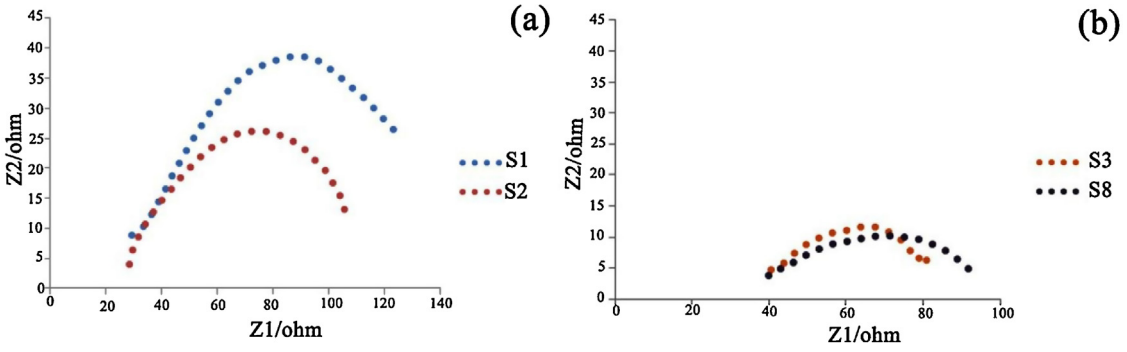

Fig. 20. EIS spectra for the DSSCs made with a) S1, S2 and b) S3, S8 electrodes, respectively.

4. Conclusions

In summary, for the first time, CdS was successfully deposited on the TiO_2 surface by different methods. The dye-synthesized solar cells were fabricated from the products. It was found that different deposition method was led to creation surfaces with different features and hence they play key roles in optical properties of the samples and solar cell performance. The fabricated solar cells made by different samples in the same conditions shown different J_{sc}, V_{oc}, FF and efficiency. It was found that SILAR technique is the best deposition method for fabrication DSSC with the best performance. In addition the crystal structure of the samples that determine the dye adsorption value is extremely dependent to the deposition method.

Acknowledgment

Authors are grateful to the council of University of Kashan for their unending effort to provide financial support to undertake this work by Grant No (159271/122)..

References

[1] B. O'Regan, M. Gratzel, Nature 353 (1991) 737–740.
[2] M. Gratzel, Nature 414 (2001) 338–344.
[3] M. Gratzel, Journal of Photochemistry and Photobiology A: Chemistry 164 (2004) 3–14.
[4] A.A. Ismail, D.W. Bahnemann, Journal of Materials Chemistry 21 (2011) 11686–11707.
[5] J.A. Rengifo-Herrera, C. Pulgarin, Solar Energy 84 (2010) 37–43.
[6] N.N. Wei, T. Han, G.Z. Deng, J.L. Li, J.Y. Du, Thin Solid Films 519 (2011) 2409–2414.
[7] S. Songara, M.K. Patra, M. Manoth, L. Saini, V. Gupta, G.S. Gowd, S.R. Vadera, N. Kumar, Journal of Photochemistry and Photobiology A: Chemistry 209 (2010) 68–73.
[8] T. Jiang, L. Miao, S. Tanemura, M. Tanemura, G. Xu, R.P. Wang, Superlattices and Microstructures 46 (2009) 159–165.
[9] H. Jia, H. Xu, Y. Hu, Y. Tang, L. Zhang, Electrochemistry Communications 9 (2007) 354–360.
[10] P.E. De Jongh, D. Vanmaekelbergh, Physical Review Letters 77 (1996) 3427–3430.
[11] G. Schlichthorl, S.Y. Huang, J. Sprague, A.J. Frank, Journal of Physical Chemistry B 101 (1997) 8141–8155.
[12] T. Bessho, E. Yoneda, J.H. Yum, M. Guglielmi, L. Tavernelli, H. Lmai, U. Rothlisberger, M.K. Nazeeruddin, M. GrÃ¤tzel, Journal of the American Chemical Society 131 (2009) 5930–5934.
[13] P.G. Bomben, K.C.D. Robson, P.A. Sedach, C.P. Berlinguette, Inorganic Chemistry 48 (2009) 9631–9643.
[14] P.G. Johansson, J.G. Rowley, A. Taheri, G.J. Meyer, S.P. Singh, A. Islam, L. Han, Langmuir 27 (2011) 14522–14531.
[15] H.C. Zhao, J.P. Harney, Y.T. Huang, J.H. Yum, M.K. Nazeeruddin, M. Gratzel, M.K. Tsai, J. Rochford, Inorganic Chemistry 51 (2012) 1–3.
[16] M. Yoshimura, Journal of Materials Research 13 (1998) 796–802.
[17] S.A. Khayyat, M. Abaker, A. Umar, M.O. Alkattan, N.D. Alharbi, S. Baskoutas, Journal of Nanoscience and Nanotechnology 12 (2012) 8453–8458.
[18] G.N. Dar, A. Umar, S.A. Zaidi, A.A. Ibrahim, M. Abaker, S. Baskoutas, M.S. Al-Assiri, Sensors and Actuators B: Chemical 173 (2012) 72–78.
[19] M. Abaker, G.N. Dar, A. Umar, S.A. Zaidi, A.A. Ibrahim, S. Baskoutas, A. Al-Hajry, Science of Advanced Materials 4 (2012) 893–900.
[20] C. Gabriel, S. Gabriel, E.H. Grant, B.S.J. Halstead, D. Michael, P. Mingos, Chemical Society Reviews 27 (1998) 213–223.
[21] H. Khallaf, I.O. Oladeji, G. Chai, L. Chow, Thin Solid Films 516 (2008) 7306–7312.
[22] H.M. Pathan, C.D. Lokhande, Bulletin of Materials Science 27 (2004) 85–111.
[23] M. Hamadanian, V. Jabbari, A. Gravand, M. Asad, Surface and Coatings Technology 206 (2012) 4531–4538.
[24] G. Anne, K. Vanmeensel, J. Vleugels, O. Van Der Biest, Colloids and Surfaces A: Physicochemical and Engineering Aspects 245 (2004) 35–39.
[25] N.G. Park, J. Van De Lagemaat, A.J. Frank, Journal of Physical Chemistry B 104 (2000) 8989–8994.
[26] W. Jarernboon, S. Pimanpang, S. Maensiri, E. Swatsitang, V. Amornkitbamrung, Thin Solid Films 517 (2009) 4663–4667.
[27] I.Y. Denisyuk, M.I. Fokina, Y. Masuda, Nanocrystals, InTech Press, 2010.
[28] J. Tauc, R. Grigorovici, A. Vancu, Physica status solidi (b) 15 (1966) 627–637.
[29] A.M. Salem, Y.A. El-Gendy, G.B. Sakr, W.Z. Soliman, Journal of Physics D: Applied Physics 41 (2008).
[30] S. Kumar, S. Kumar, P. Sharma, V. Sharma, S.C. Katyal, Journal of Applied Physics 112 (2012).
[31] S. Baskoutas, P. Poulopoulos, V. Karoutsos, M. Angelakeris, N.K. Flevaris, Chemical Physics Letters 417 (2006) 461–464.
[32] P. Poulopoulos, S. Baskoutas, S.D. Pappas, C.S. Garoufalis, S.A. Droulias, A. Zamani, V. Kapaklis, The Journal of Physical Chemistry C 115 (2011) 14839–14843.
[33] Y. Guo, N.H. Lee, H.J. Oh, C.R. Yoon, K.S. Park, W.H. Lee, Y. Li, H.G. Lee, K.S. Lee, S.J. Kim, Thin Solid Films 516 (2008) 8363–8371.
[34] M.C. Kao, H.Z. Chen, S.L. Young, C.Y. Kung, C.C. Lin, Thin Solid Films 517 (2009) 5096–5099.
[35] Z.S. Wang, H. Kawauchi, T. Kashima, H. Arakawa, Coordination Chemistry Reviews 248 (2004) 1381–1389.
[36] R. Katoh, A. Furube, A.V. Barzykin, H. Arakawa, M. Tachiya, Coordination Chemistry Reviews 248 (2004) 1195–1213.
[37] J.R. Durrant, S.A. Haque, E. Palomares, Coordination Chemistry Reviews 248 (2004) 1247–1257.
[38] P.Y. Chen, C.P. Lee, R. Vittal, K.C. Ho, Journal of Power Sources 195 (2010) 3933–3938.
[39] X. Yong, M.A.A. Schoonen, American Mineralogist 85 (2000) 543–556.